Eng. Sci., 2022, **18**, 253–262

Engineered Science
DOI: https://dx.doi.org/10.30919/es8d667

Performance Analysis of a Standalone Photovoltaic Battery Based Mixer Grinder

Deekshitha S. Nayak* and R. Shivarudraswamy*

Abstract

A standalone solar photovoltaic system with battery storage for a mixer grinder has been presented in this paper. The proposed brushless direct current (DC) mixer grinder is designed for access in remote areas with increased efficiency and reduced complexity. In this system, the control architectures and standard hardware implementation ensure easy service, maintenance, and installation. The switching voltage source inverter reduces the power loss and eliminates the phase current sensors by using this control algorithm. In this system additional control circuit is not required to regulate the speed of the brushless DC motor used to run the mixer grinder, it reduces the overall cost. The proposed mixer grinder system performance is not affected under dynamic conditions. The proposed system is demonstrated practically and validated with simulation results using matrix laboratory (MATLAB)/Simulink. It can be seen that the energy saved per annum over a conventional mixer grinder is 153.3 KWh.

Keywords: Mixer grinder; Solar photovoltaic array; Bidirectional charge control; Battery; Boost converter; Voltage source inverter.
Received: 18 November 2021; Revised: 02 March 2022; Accepted: 05 March 2022.
Article type: Research article.

1. Introduction

Diminishing non-renewable resources and growth in energy demand have promoted widespread research in the field of renewable energy generation, *i.e.*, wind and solar-based technologies.[1] In most applications, a solar photovoltaic array is used due to its less maintenance and abundant availability.[2] To overcome energy scarcity and demand, the use of energy-efficient appliances is gaining interest.[3] The system uses a direct current (DC) motor, induction motor, or universal motor in household appliances.[4] Mixer grinders are commonly used in all homes.[5] Almost all mixer grinders use the universal motor as a driving motor. Their input power ratings range from 400 to 750 watts. The mixer grinder's 420 W universal motor delivers 280 W mechanical power, with around 100 W lost as windage losses due to the fan necessary for cooling. As a result, the motor only produces 180 W of useful shaft power, resulting in 43% efficiency. Furthermore, the current mixer grinders are extremely noisy.[6] The universal motor is driven by the simple controller[7] using an alternating current supply.[8] The efficiency of the universal motor is less due to the presence of brushes and a mechanical commutator.[9] Besides, they consume more power because of no ease of control for fixed speed or other programmable performance features.[10,11] There is research on the applications of mixer grinders that focuses on applications such as improving motor performance and torque density.[12,13]

The mixer grinder requires high efficiency, high speed, good speed control, and good torque characteristics.[14] So the proposed motor is an efficient substitute for the mixer grinders that are currently available. It would decrease the requirement of peak power, which will enable the user to function as a mixer grinder directly from renewable resources. The motor has an output power of 80 watts, which is equivalent to a 500-watt universal motor currently in use in the mixer grinder. The aim of this work is to design a low-power consumption and highly efficient mixer grinder which is useful in rural India where power is limited and the connected load is less than 200 W.

2. Designing of the proposed system

This paper focuses on the low power consumption and mixer grinder system with higher efficiency. So the proposed system is the solar photovoltaic array, a battery-based brushless DC motor-driven mixer grinder. Solar photovoltaic array power generation is irregular, making interrupting the mixing of the

Department of Electrical and Electronics Engineering, Manipal Institute of Technology, Manipal Academy of Higher Education, Manipal, 576104, Karnataka, India.
**E-mail:* deekshitha.nayak06@gmail.com (D. Nayak), shivarudraswamy.r@manipal.edu (R. Shivarudraswamy)
#*These authors contributed to this work equally.*

ingredients possible. Solar photovoltaic array power is insufficient to run the mixer grinder system when the weather is bad or at night. So, a battery is coupled with a solar photovoltaic (SPV) array for the continuous flow of power. The control of power flow for charging/discharging battery energy storage is through the bi-directional DC-DC converter. As per the solar photovoltaic array power and load requirement, the battery gets charged or discharged and an external power supply is not required. A common capacitor enables the bi-directional power flow at the DC bus of a voltage source inverter. For economical driving, the phase current sensors are eliminated. The maximum power point tracking of the solar photovoltaic array is gained by the modified perturb and observer algorithm using a boost converter.

An operating voltage source inverter controls the stator current of the brushless DC motor in pulse width modulation for a predefined interval. The voltage source inverter functions in fundamental frequency to minimize the switching loss. For the variable speed drive for the brushless DC motor, speed regulated by the outer loop and current regulated by the inner loop anti-windup proportional-integral (PI) controller has been used. The difference between the saturated output and the unsaturated input is the anti-windup PI controller input to the integrator. It has a better performance than a conventional PI controller. The hybrid solar photovoltaic array–Battery-based brushless DC motor-driven mixer grinder system is simulated in MATLAB/Simulink and experimental validation is demonstrated.

A schematic diagram of the proposed hybrid mixer grinder system is displayed in Fig. 1. The solar photovoltaic array with a boost converter and battery with a bidirectional converter is coupled with the DC bus. The brushless DC mixer grinder is associated with a common DC bus by a voltage source inverter. The boost converter is engaged to function maximum power point tracking of the solar photovoltaic array by a perturb and observer algorithm and the buck-boost converter acts as the charge controller for the battery. The mixer grinder is coupled with a shaft of the brushless DC motor with three inbuilt Hall effect sensors to produce Hall signals for commutation. The speed and current anti-windup PI controller with the Hall signals are used for the switching of the voltage source inverter. Table 1 shows the comparison with the various batteries specifications and it can be concluded that lead acid is preferred for the proposed system because of its less cost, good overcharge tolerance, and less maintenance.

2.1 Photovoltaic array

A 4-pole 4300 rpm brushless DC motor is used to drive an 80 W mixer grinder. The cost-effective solar photovoltaic array and battery are used. The design parameters of the solar photovoltaic array are given in Table 2. The peak power capacity of the solar photovoltaic array is 40 W and is designed with 19GCLVOAA012431 modules, and a 24 V, 8 Ah lead-acid battery is connected to provide power to the mixer grinder when there is no grid power.

The perturb and observe algorithm is used as the maximum power point tracking to extract maximum power from the photovoltaic array. In this method, because of the nonlinear property of the photovoltaic voltage and current, the power from a photovoltaic array tracks the maximum power point of the curve. The tracker works by intermittently decrementing or incrementing the voltage of a photovoltaic array by constantly tracking the power of the photovoltaic.[15,16] The modification of conventional perturb and observation maximum power point tracking is attained by comprising the aspect of

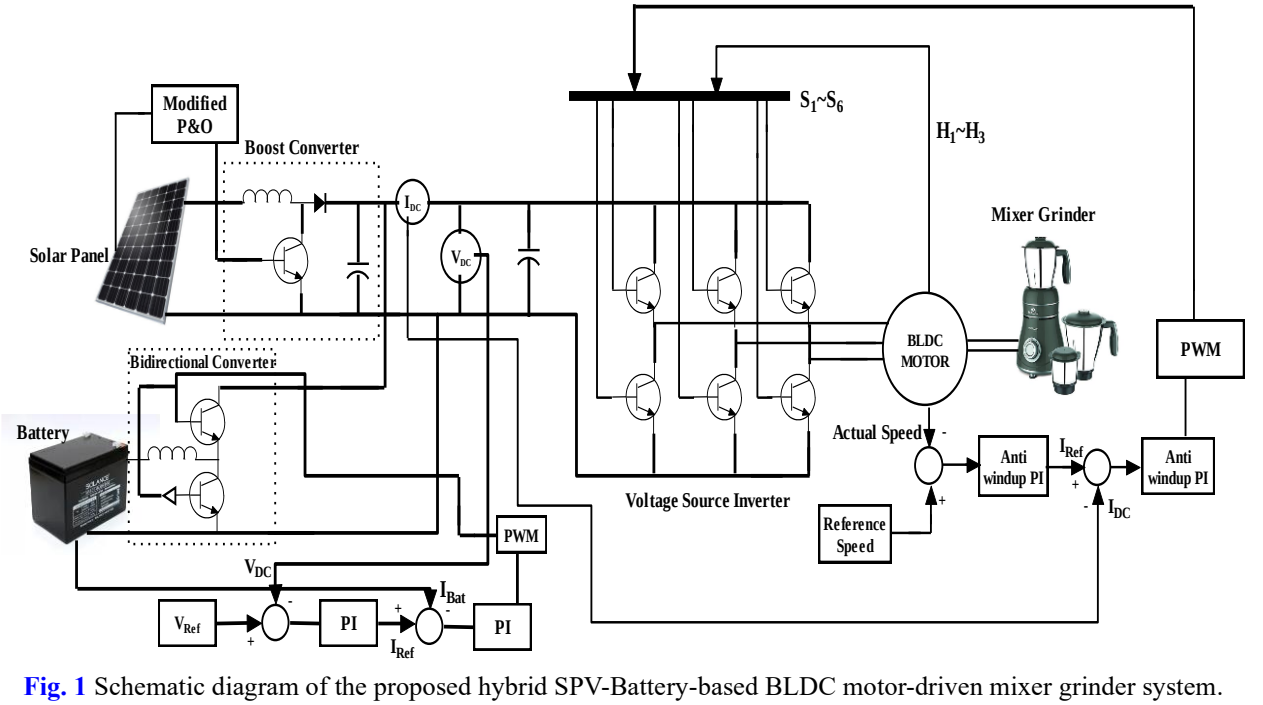

Fig. 1 Schematic diagram of the proposed hybrid SPV-Battery-based BLDC motor-driven mixer grinder system.

Table 1. Comparison with the different batteries.

Specifications	Lead Acid	NiCd	NiMH	Li-ion Cobalt	Li-ion Manganese	Li-ion Phosphate
Specific Energy Density (Wh/Kg)	30-50	45-80	60-120	150-190	100-135	90-120
Internal Resistance (mΩ)	<100 12V pack	100-200 6V pack	200-300 6V pack	150-300 7.2V	25-75[2] Per cell	25-50[2] Per cell
Cycle Life (80% discharge)	200-300	1000[3]	300-500[3]	500-1000	500-1000	1000-2000
Overcharge Tolerance	High	Moderate	Low	Low	Low	Low
Cell Voltage	2V	1.2V	1.2V	3.6V	3.8V	3.3V
Charge Temperature	-20-50 °C	0-45 °C	0-45 °C	0-45 °C	0-45 °C	0-45 °C
Discharge Temperature	-20-50 °C	0-65 °C	0-65 °C	0-60 °C	0-60 °C	0-60 °C

Table 2. Design of the SPV array.

Parameters	PV module (19GCLVOAA012431)
N_s	36
Open circuit voltage, V_{oc}	22.12V
Short circuit current, I_{sc}	1.19A
The voltage at MPP, V_{mp}	18.25V
Current at MPP, I_{mp}	1.12A
Modules in series, N_s	V_{mp}/V_m = 18/18.25 = 1
Modules in parallel, N_p	I_{mp}/I_m = 2.2/1.12 = 2
Peak Power	40W

current variations (ΔI_{PV}) along with power variation (ΔP_{PV}) and voltage variation (ΔV_{PV}), which improves the drift problem with an adaptive perturbation step size that reduces the steady-state oscillation.[17]

2.2 Charging control of the battery

The bidirectional DC-DC converter is used for the power flow between the battery and the DC bus depicted in Fig. 2. The DC bus voltage is regulated to 24 V using the voltage regulator. The current regulator is used to control the battery current and charging/discharging of the battery. The outer loop is the voltage and the inner loop is the current. The proportional-integral (PI) controller is used as a voltage and current regulator. The current regulator sends the pulse width modulation pulses to the gates of the bidirectional converter.

The overall control function is given as:

$$u(t) = K_p e(t) + K_i \int_0^t e(\tau)d\tau \quad (1)$$

where K_p is the proportional gain, K_i is the integral gain, e(t) = SP-PV(t) is the error of set, e(t) = SP-PV(t) is the error of set point and process variable, t is the instantaneous time and τ is the variable of integration.

In the design of the PI controller, the transient requirement is given as

$$t_r = \frac{1.8}{\omega_n} \quad (2)$$

Steady-state requirement is e_{ss} = 0 and the controller design is given as

$$D(s) = K_p + \frac{K_i}{s} \quad (3)$$

The values of K_p = 0.56 and K_i = 0.025 are selected.

2.3 Electronic commutation of the BLDC motor

The electronic commutation indicates the current flowing through the brushless DC motor windings such that a symmetrical direct current is drawn from the DC bus of the voltage source inverter and employed at the mid-of-back EMF (electromotive force). The Hall signals are transformed into fundamental frequency (S_1-S_6) using the decoder circuit and summed up with the pulse width modulation signals to generate six pulses to the voltage source inverter. To reduce the switching loss, the voltage source inverter is switched in the pulses of the fundamental frequency.

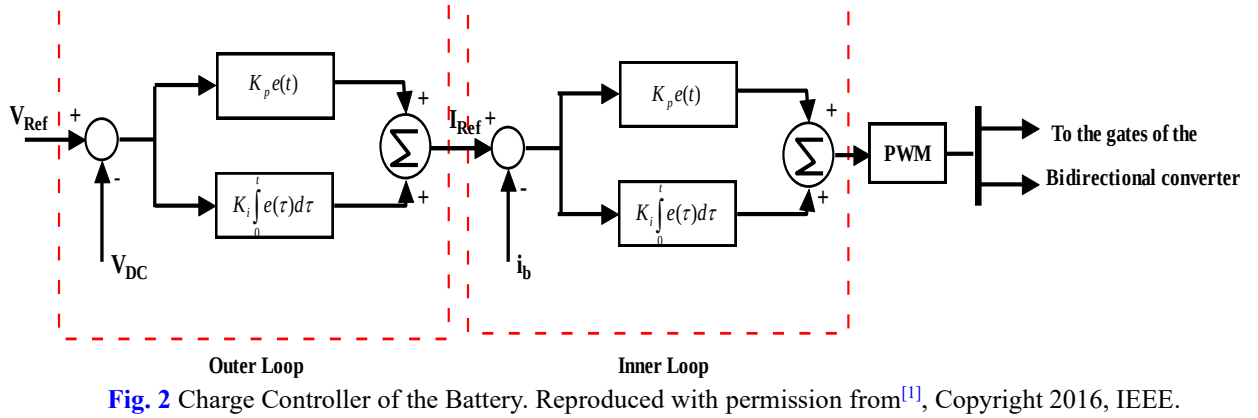

Fig. 2 Charge Controller of the Battery. Reproduced with permission from[1], Copyright 2016, IEEE.

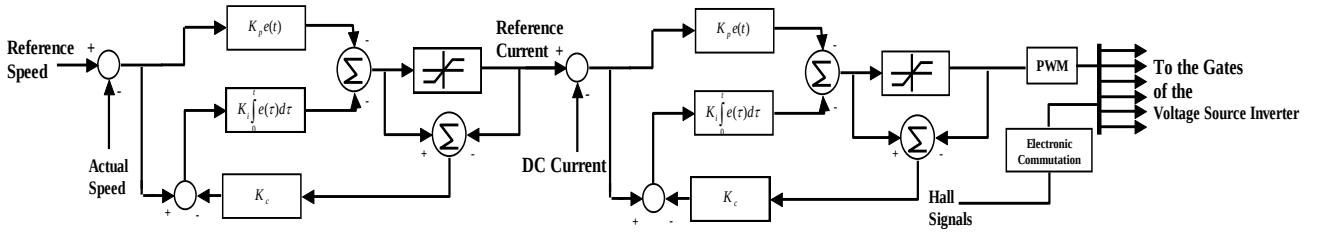

Fig. 3 Speed Controller for the BLDC motor.

The speed control of the brushless DC motor can be seen in Fig. 3. The outer loop is the speed regulator and the inner loop is the current regulator. The saturation characteristics of BLDC motor drives using PI control and pulse width modulation schemes are significant, resulting in the windup phenomenon. It is a condition in which there is a substantial change in set point and the integral term has to store (accumulate) a considerable mistake during the increase. Overshooting occurs when a considerable amount of error accumulates, and it continues to expand while the accumulated error is unwound solely by errors in the other direction. As a result, overshoot and settling time are a unique challenge to a traditional proportional integral derivative (PID) controller. Instead of a PI controller, an anti-windup PI controller has been used. The difference between the saturated output and the unsaturated input is the anti-windup PI controller input to the integrator. It has a better performance than a conventional PI controller.

The overall control function is

$$u(t) = K_p e(t) + K_i \int_0^t e(\tau)d\tau + K_c \quad (4)$$

where K_p is the proportional gain, K_i is the integral gain, e(t) = SP-PV(t) is the error of set point and process variable, t is the instantaneous time and τ is the variable of integration, K_c is the anti-windup gain, K_c is inversely proportional to the proportional gain.

The design of the speed controller and the current controller is given as

$$D(s) = K_p + \frac{K_i}{s} + K_c \quad (5)$$

In the speed loop, $K_p = 0.5$, $K_i = 0.01$, $K_c = 2$, and in the current loop, $K_p = 0.95$, $K_i = 0.09$, $K_c = 1.05$.

Table 3. Switching pulse generation of the voltage source inverter.[1]

Rotor Position	Hall Signals			Active Switches
$\theta(\omega)$	H_3	H_2	H_1	
0-60	1	0	1	S_1; S_4
60-120	0	0	1	S_1; S_6
120-180	0	1	1	S_3; S_6
180-240	0	1	0	S_2; S_3
240-300	1	1	0	S_2; S_5
300-360	1	0	0	S_4; S_5

The rotor position is detected by the Hall sensors at the interval of 60°. To reduce the switching loss, the voltage source inverter is switched in the pulses of the fundamental frequency only two switches at a time as shown in Table 3.

The DC-link capacitor of the voltage source inverter is designed as follows. The fundamental frequency output of the voltage source inverter corresponding to the brushless DC motor-rated speed ω_{rated} is given by:

$$\omega_{rated} = 2\pi f_{rated} = 2\pi \frac{N_{rated} P}{120} \quad (6)$$

where f_{rated} are the rated fundamental frequencies of the voltage source inverter output voltage, P is the number of poles, and N_{rated} is the rated speed of a brushless DC motor.

The fundamental frequency output of the voltage source inverter corresponding to the lowest speed of the brushless DC motor is vital for the mixer grinder.

$$\omega_{min} = 2\pi f_{min} = 2\pi \frac{NP}{120} \quad (7)$$

where f_{min} are the fundamental frequencies of the voltage source inverter output voltage, N is the minimum speed of a brushless DC motor, and P is the number of poles of a brushless DC motor.

The DC-link-rated capacitor value C_{rated} is given as

$$C_{rated} = \frac{I_{DC}}{6\omega_{rated}\Delta V_{DC}} \quad (8)$$

where ω_{rated} is the rated speed of the brushless DC motor (rad/sec), I_{DC} is the DC bus current, ΔV_{DC} is the small change in DC bus voltage.

The DC-link minimum capacitor value C_{min} is given as

$$C_{min} = \frac{I_{DC}}{6\omega_{min}\Delta V_{DC}} \quad (9)$$

The value of the DC link capacitor selected is 250 μ F.

where C_{min} is the minimum capacitor value, ω_{min} is the minimum speed of the brushless DC motor (rad/sec), I_{DC} is the DC bus current, ΔV_{DC} is the small change in DC bus voltage.

The proportionality constant K for the mixer grinder is given as:

$$K = \frac{P}{\omega_r{}^3} \quad (10)$$

where P = 80W is the rated power of the brushless DC motor and ω_r is the mechanical rated speed of the brushless DC motor in rad/sec.

The switching pattern of the voltage source inverter is shown in Table 3. Only two switches are turned on at a particular instant of time to minimize the switching loss. Fig. 4 shows the state space representation of the pulse width modulation. V_1 to V_6 are the switching state of the voltage source inverter. The 1 indicates the switch is on state and 0 indicates the switch is off state. T_1 and T_2 is the time period of interval 1 and 2, T_{Ref} is the reference time period and α is

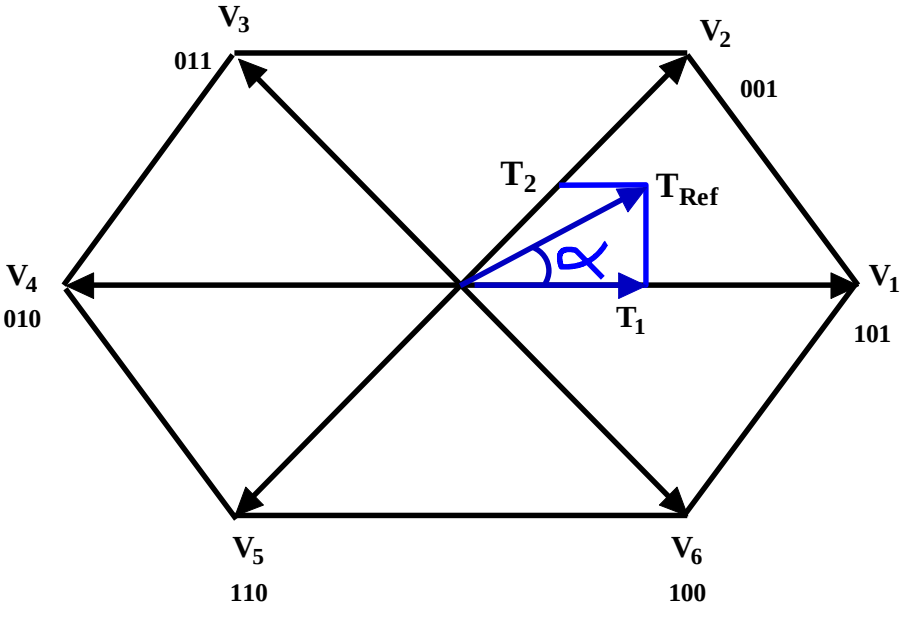

Fig. 4 State space representation of the PWM.

the angle of the time period. The magnitude of this vector is proportional to the output voltage's magnitude, and the time it takes for this vector to complete one revolution is the same as the output voltage's fundamental time period. There are six non-zero voltage vectors (V_1-V_6) and these vectors form the regular hexagon. The time periods T_1 and T_2 are for the vectors V_1 and V_2, and $0 < m < 0.9$ is the modulation index.

$$T_1V_1 + T_2V_2 = V \quad (11)$$

$$T_1 + T_2 + T_0 = T_{Ref} \quad (12)$$

3. Results and Discussion

The solar photovoltaic array with a maximum of 40 W output with the battery capacity was considered to be 24 V, 8 Ah, and the speed of the brushless DC motor in the mixer grinder was chosen as 4300 rpm. As the mixer grinder is operated with a solar photovoltaic system, if sufficient solar radiation is not available, it will run with battery power which will be stored when the sunlight is available. The performance of both simulation and hardware results of solar photovoltaic–battery-based mixer grinder with brushless DC motor are presented here.

The experimental setup of the proposed system can be seen in Fig. 5. The solar panel with the maximum power point tracking controller used to extract the maximum power from the panel is connected to the boost converter and then fed to the DC bus. When the generated power from the panel exceeds the load power, the excess power can be stored in the battery. The DC bus is coupled with the battery using the bidirectional converter.

The three-phase brushless DC motor is connected to the voltage source inverter which is connected to a DC bus. The grinder jar is connected to the brushless DC motor shaft embedded with the blades. The motor speed can be changed using a rotary switch. The mixer grinder can be run at low, medium, and high speeds. The microcontroller ATMEGA 2560 is used as a control unit in the proposed system. Table 4 depicts the design parameters of the boost converter, battery, bidirectional converter, and also brushless DC motor of the proposed system.

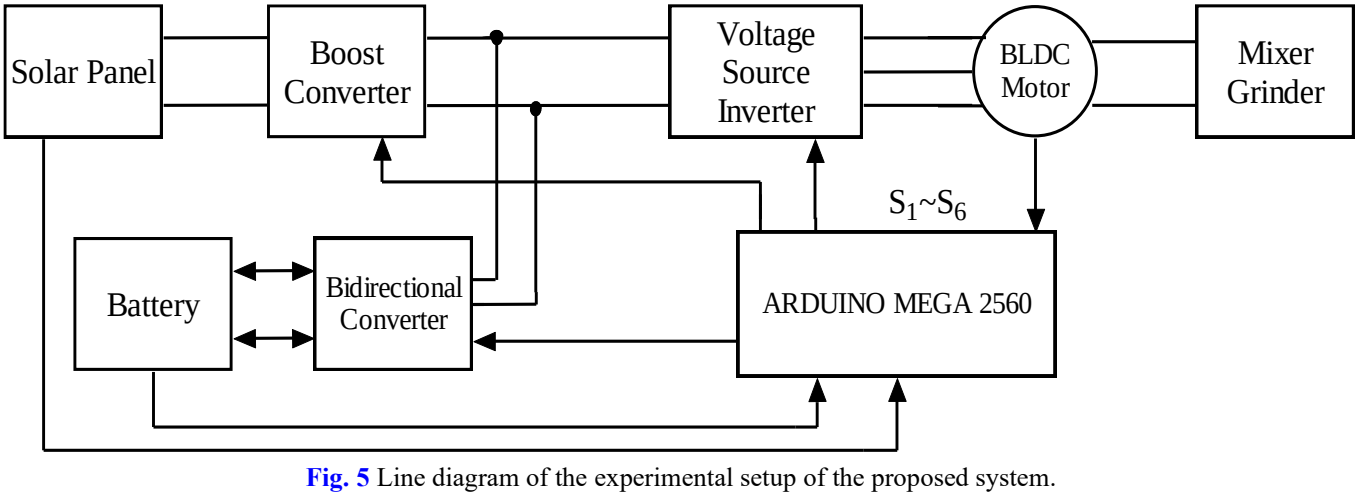

Fig. 5 Line diagram of the experimental setup of the proposed system.

Table 4. Design of the parameters used in the proposed system.

Boost converter	BLDC motor	Battery
Duty cycle D $= \frac{V_{DC}-V_{PV}}{V_{DC}} = \frac{24-18}{24} = 0.25$	Rated speed = 4300 rpm	Type of Battery = Sealed Lead Acid
Inductor Current $I_L = N_P I_m = 2 * 1.12 = 2.24A$	Number of poles = 4	Nominal Voltage = 24V
Inductor L $= \frac{D*V_{PV}}{f_{SW}*10\%I_L} = 1mH;$	Stator resistance = 0.37Ω	Rated Capacity = 8Ah
Capacitor C $= \frac{I_{DC}}{6*\omega*\Delta V_{DC}} = 700\mu F$	Stator inductance = 1 mH	Bidirectional converter: Inductor = 0.7mH

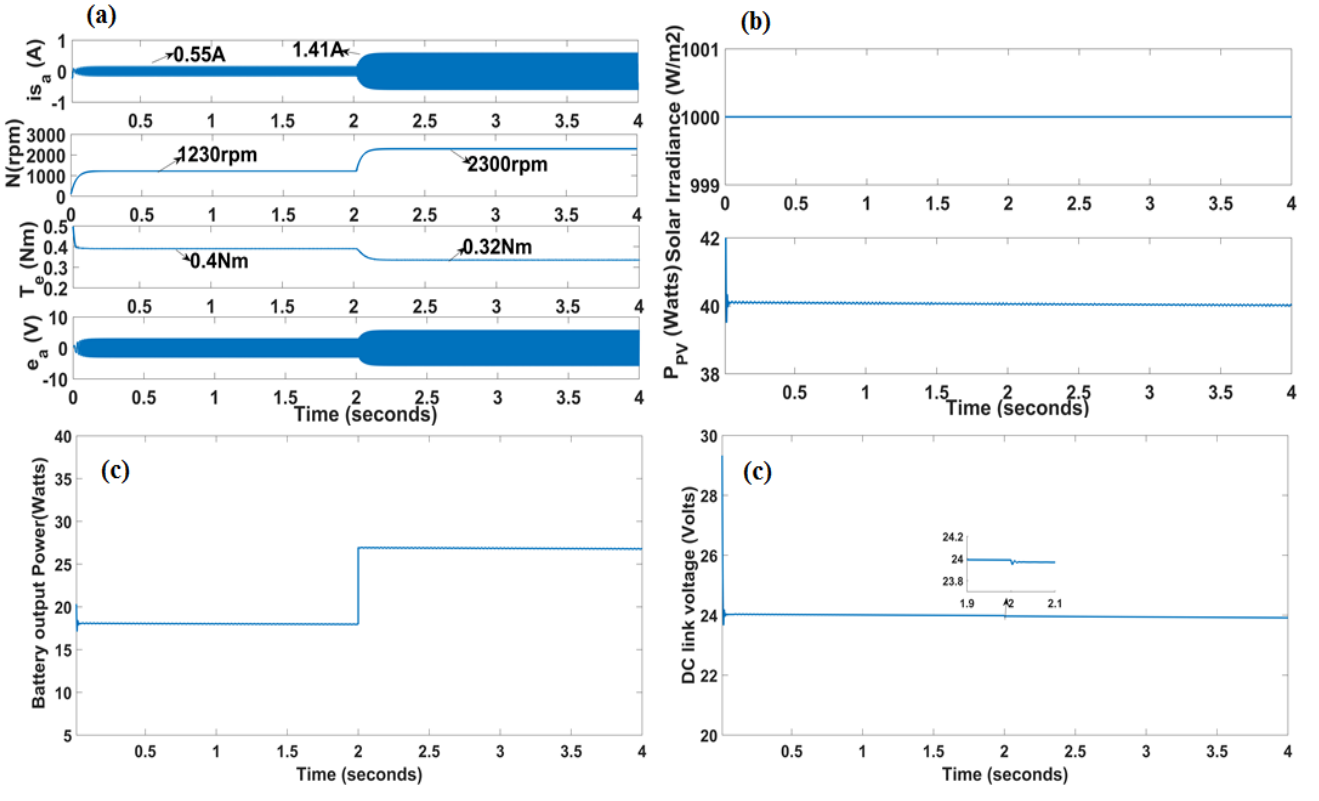

Fig. 6 Dynamic performance of the proposed system (a) brushless DC motor (b) PV (c) Battery and DC bus.

The dynamic performance of the proposed system can be seen in Fig. 6. The simulation has been carried out at two motor speeds, one at 1230 rpm and another at 2300 rpm and the simulation is done for 4 seconds. The solar irradiance is taken at 1000 W/m^2, and the dynamic variations of the photovoltaic array, battery, and brushless DC motor are presented in Fig. 6. The power consumed by the load at 1230 rpm is 58 W; similarly, power consumed by the load at 2300 rpm is 67 W at half load which is considered here. The output power from the SPV at half load is 40 W can be seen in Fig. 6b and the remaining power taken from the battery is 18 W at 1230 rpm and 27 W at 2300 rpm as shown in Fig. 6c to meet the total load power. In the DC link voltage, a slight drop at 2 seconds due to the sudden change in the speed can be observed in Fig. 6c. The motor current increases as the speed changes from 1230 rpm to 2300 rpm can be observed in Fig. 6a. And also Fig. 6a shows that the electromagnetic torque changes from 0.4 Nm to 0.32 Nm when speed changes from 1230 rpm to 2300 rpm. It can be observed that when the speed of the motor increases the torque decreases. Also, it can be observed that from Fig. 6a there is an increase in back emf with a change in the speed of the motor from 1230 rpm to 2300 rpm. Fig. 6c shows the power taken by the load from the battery when the speed changes from 1230 rpm (0 to 2 seconds) to 2300 rpm (from 2 seconds to 4 seconds).

Figure 5 shows the hardware components of the proposed system and Fig. 7 shows the dynamic performance of hardware implementation. In the hardware part, two motor speeds (1230 rpm & 2300 rpm) are considered as in the simulation part at half load. In Fig. 7a, it can be observed that the current of the motor increases due to a change in speed from 1230 rpm to 2300 rpm. The stator current of the motor is 0.53 A for 2 seconds when the motor runs at 1230 rpm and the stator current is 1.32 A after 2 seconds when the motor speed is 2300 rpm. The torque of the motor decreases and back emf increases with an increase in speed from 1230 rpm to 2300 rpm can be observed in Fig. 7a. The electromagnetic torque changes from 0.4 Nm to 0.32 Nm with a change in speed from

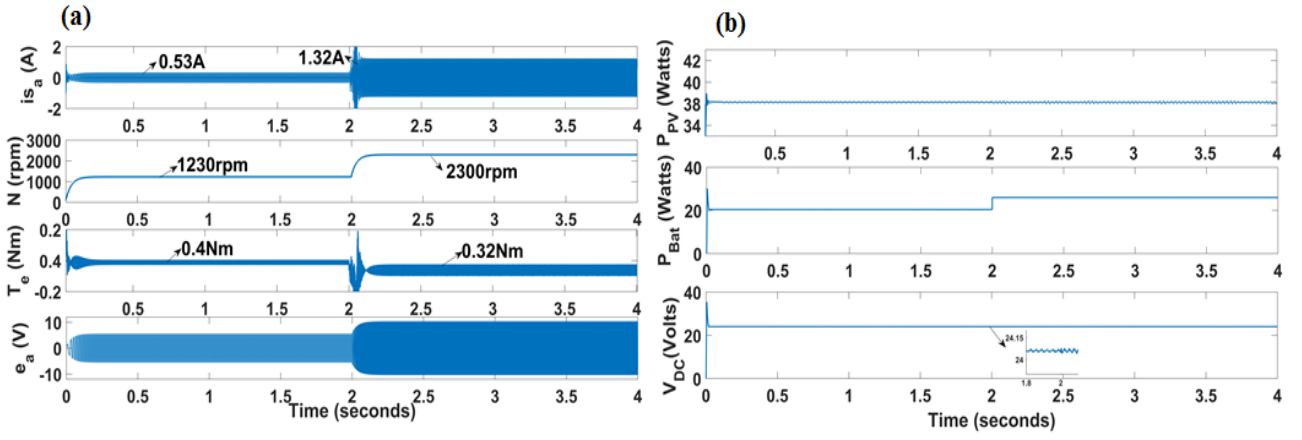

Fig. 7 Hardware performance of the proposed system (a) Brushless DC motor (b) PV, Battery, and DC bus.

Table 5. Comparison of both simulation and hardware results.

Parameters	Speed 1 (1230 RPM)		Speed 2 (2300 RPM)	
	Simulation	Hardware	Simulation	Hardware
Solar PV Output (1000W/m^2)	40W	38W	40W	38W
Battery Output	18W	20W	27W	29W
DC Link Voltage	24V	24V	24V	24V
Stator Current	0.55A	0.53A	1.41A	1.32A
Efficiency (No load)	78.9%	78.4%	79.8%	79.5%
Efficiency (Half load)	75.6%	75.1%	77.1%	76.8%

1230 rpm to 2300 rpm. The solar irradiance is taken at 1000 W/m^2 and the power of the photovoltaic array and battery are listed in Fig. 7b. The power flow pattern has been observed and it is measured using the flux meter and it can be seen from Fig. 7b. The power flow pattern of the mixer grinder at 50% load runs at two different speeds (1230 rpm and 2300 rpm). In practice, the total power consumed by the mixer grinder at half load at 1230 rpm is 58 W with 1000 W/m^2, power from the solar photovoltaic is 38 W, and the remaining power 20 W is taken from the battery. Similarly, the power consumed by the mixer grinder at the speed of 2300 rpm at half load is 67 W, and the remaining 29 W is taken from the battery which is charged at load condition.

Different parameters are compared with the simulation and hardware results for the two speeds seen in Table 5. For the 1000 W/m^2 solar irradiance, the output obtained from the solar PV in the simulation is 40 W, and hardware is 38 W, and the remaining power is obtained from the battery to meet the load. The efficiency at no load condition and/or half load is slightly higher in the simulation compared to hardware as shown in Table 5. The results of the simulation and hardware are almost similar as per the no-load and load conditions.

Table 6 shows the comparison of the grinding time of food material for both conventional and proposed mixer grinders in the experimental setup. The specification considered in the conventional mixer grinder is 230 V, 500 W rating with 20000 rpm rated speed. The food material used for the grinding is split chickpea lentils (chana dal) for both conventional and proposed systems, for grinding the food material is considered with 50% load (1 L). The grinding time of the proposed mixer grinder is compared with the conventional system that has been noted down. It can be observed that the proposed mixer grinder works more efficiently compared to the conventional mixer grinder system because the quality of the grinding material is better in the proposed mixer grinder even at low power compared to the conventional mixer grinder. However, the grinding time of the proposed system is slightly longer and the speed level is lower compared to the conventional mixer grinder, as mentioned in Table 6.

Table 6. Comparison of grinding time of the conventional and proposed mixer grinder system.

Split chickpea lentils (Chana Dal) (50% of the 1L jar)	Conventional Mixer Grinder (500W)	Proposed Mixer Grinder (80W)
Speed 1	25 sec (13268 RPM)	40 sec (1230 RPM)
Speed 2	18 sec (15865 RPM)	21 sec (2300 RPM)

The efficiency of the commercially available conventional mixer grinder of rating 500 W (Philips model) and the proposed brushless DC mixer grinder has been measured using a flux energy meter. In Fig. 8, the efficiency of the existing conventional mixer grinder is 53.15% at the no-load condition and 49.63% at the half-load condition.[9] In the proposed mixer grinder, the efficiency is 79.5% at the no-load condition and 76.8% at the half-load condition.

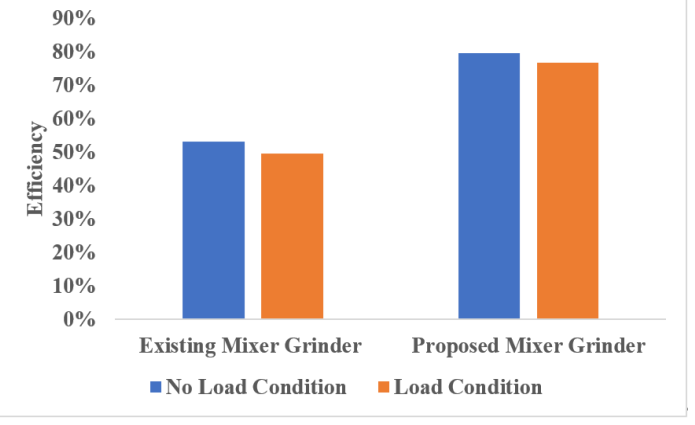

Fig. 8 Efficiency comparison of the existing and proposed mixer grinder.

The payback period of the proposed motor is calculated without considering the cost of the photovoltaic systems, battery and other components can be observed in Table 7. The market-available mixer grinder uses a universal motor with a power rating of 500 W and the proposed mixer grinder uses a brushless DC motor with a power rating of 80 W. The payback period of the proposed motor is 1.7 years.

Table 8 shows the summary of the relevant literature papers in comparison with this present work. It can be observed that in this work highly efficient motor is used in the mixer grinder application and a control scheme is designed which improvises the grinding performance.

4. Conclusions

A solar photovoltaic array with a battery-fed low-power mixer grinder is proposed and demonstrated through simulation and experimental validation. The proposed system is designed and modeled systematically and its performance is analyzed. The voltage source inverter is switched in the fundamental switching frequency to reduce the switching loss. The complexity and overall cost of the proposed mixer grinder using a brushless DC motor are reduced by eliminating phase current sensors and an additional circuit in the speed control. The grinding quality in the proposed mixer grinder is improved compared to the conventional mixer grinder and also increases in efficiency by 26%. The payback period of the proposed motor is 1.7 years.

Acknowledgments

The mixer grinder with low power Solar Photovoltaic battery based has been applied for an Indian patent. Application no: 202041046109 filed on 22nd October 2020.

Conflict of interest

There are no conflicts to declare.

Supporting information

Not applicable.

Table 7. Payback period of the proposed motor.

Motor Rating	500W/4P	80W/4P
Rated Voltage	230V AC	24V DC
Motor loading in percentage	100%	100%
Efficiency	52.13%	86.4%
Power Tariff	5 INR/KWh	5 INR/KWh
Operation of the motor per annum	365	365
Energy consumption per annum	182.5KWh	29.2KWh
Energy saved per annum over conventional mixer grinder		153.3KWh
Annual Energy Bill	547.5 INR	87.6 INR
Saving towards Energy bill per annum		459.9 INR
Purchase price of the motor (Exclude taxes and duties)	4200 INR	5000 INR
Increment investment over a standard motor		800 INR
Payback of increment investment		1.739 years

Table 8. Summary of the relevant literature with the present work.

Paper	Method used	Type of Motor	Ratings	Efficiency	Load Characteristics	Critical Outcome
[8,9]	Mathematical Modelling	Universal Motor	500 W/230 V AC	39.6% - 51.8%	Yes	Commercially available mixer grinder is very less efficient.
[5]	Finite Element Analysis	Ferrite Magnet Brushless DC Motor	200 W/48 V DC	70%	No	Merely Software design is presented.
[18]	Finite Element Analysis	Switched Reluctance Motor	280 W/3 Phase	68%	No	Software design is presented.
[19]	Discrete Element Modelling	No	20 RPM	No	Yes (Initial Load Pattern)	As the filling in the jar increases, the grinding performance is significantly reduced.
[20]	FTIR Technique/ SEM image	MXene# (MX-B)	300 W	No	No	Blender made up of MXene# is highly efficient.
This Paper	MATLAB and Hardware	PM Brushless DC Motor	80 W/24V	76.8%-79.5%	Yes	The proposed mixer grinder is low-power and highly-efficient along with improved grinding performance.

Note: MXene#: Two-dimensional inorganic compounds.

References

[1] R. Kumar, B. Singh, *IEEE 1st International Conference on Power Elect., Intelligent Control and Energy Systems*, 2016, 1-6, doi: 10.1109/ICPEICES.2016.7853662.

[2] A. K. Singh, I. Hussain, B. Singh, *IEEE International Conference on Industrial Electronics for Sustainable Energy Systems*, 2018, 320-325, doi: 10.1109/IESES.2018.8349896.

[3] B. Jong Nam, Grace Firsta Lukman, Jin Woo Ahn, Dong-Hee Lee, *IET Electric Power Applications*, 2020, **14**, 2154-2162, doi: 10.1049/iet-epa.2020.0078

[4] D. Kamalakannan, N. Jeyapaul Singh, M. Karthi, V. Narayanan, N. S. Ramanathan, *First International Conference on Sustainable Green Buildings and Communities*, 2016, 1-6, doi: 10.1109/SGBC.2016.7936063.

[5] V. Gholase, B. G. Fernandes, *IEEE International Conference on Industrial Technology*, 2015, **1**, 696-701, doi: 10.1109/ICIT. 2015.7125179.

[6] H. Xu, K. King, Y. Jani, *IEEE Annual Meeting of Industry Applications*, 2007, **1**, 701-705, doi: 10.1109/07IAS.2007.111.

[7] S. B. Kjaer, J. K. Pedersen, F. Blaabjerg, *IEEE Transactions on Industry Applications*, 2005, **41**, 1292-1306, doi: 10.1109/tia.2005.853371.

[8] N. Deekshitha, R. Shivarudraswamy, *IEEE International Conference on Automatic Control and Intelligent Systems,* 2018, **1**, 105-110, doi: 10.1109/I2CACIS.2018.8603693.

[9] N. Deekshitha and R. Shivarudraswamy, *IEEE International Conference Electrical Engineering Congress*, 2020, **1**, 1-4, doi: 10.1109/iEECON 48109.2020. 229457.

[10] G. Papa, B. Korousic-Seljak, B. Benedicic, T. Kmecl, *IEEE Transactions on Industrial Electronics*, 2003, **50**, 602-611, doi: 10.1109/tie.2003.812455.

[11] M. A. G. de Brito, L. Galotto, L. P. Sampaio, G. de Azevedo e Melo, C. A. Canesin, *IEEE Transactions on Industrial Electronics*, 2013, **60**, 1156-1167, doi: 10.1109/tie.2012.2198036.

[12] R. Otero, A. Miguel and E. O'Neill-Carrillo, *IEEE Energy 2030 Conference*, 2008, 1-6, doi: 10.1109/ENERGY. 2008.4781006.

[13] S. Mehdi, A. Aghajani, S. Shabani, J. Jamali, *Energy Equipment and Systems*, 2015, **3**, 57-71, doi: 10.22059/EES.2015.13911.

[14] D. Bhagat Chinma, S. P. Nikam, B. G. Fernandes, *First International Conference on Sustainable Green Buildings and Communities*, 2016, **1**, 1-6, doi: 10.1109/SGBC.20 16.7936065.

[15] D. F. Teshome, C. H. Lee, Y. W. Lin, K. L. Lian, *IEEE Journal of Emerging and Selected Topics in Power Electronics*, 2017, **5**, 661-671, doi: 10.1109/jestpe.2016.2581858.

[16] B. Subudhi, R. Pradhan, *IEEE Transactions on Sustainable Energy*, 2013, **4**, 89-98, doi: 10.1109/TSTE.2012.2202294.
[17] D. Sera, L. Mathe, T. Kerekes, S. V. Spataru, R. Teodorescu, *IEEE Journal of Photovoltaics*, 2013, **3**, 1070-1078, doi: 10.1109/jphotov.2013.2261118.
[18] S. Ekram, N. Ravi, K. R. Rajagopal, D. Mahajan, *IECON 2007-33rd Annual Conf. of the IEEE Industrial Electronics Society*, 2007, 193-197, doi: 10.1109/IEC ON.2007.4460046.
[19] K. Sen, N. Velez, C. Anderson, J. K. Drennen, A. S. Zidan, B. Chaudhuri, *International Journal of Pharmaceutics*, 2020, **578**, 119131, doi: 10.1016/j.ijpharm.2020.119131.
[20] V. Thirumal, R. Yuvakkumar, P. S. Kumar, S. P. Keerthana, G. Ravi, D. Velauthapillai, B. Saravanakumar, *Chemosphere*, 2021, **281**, 130984, doi: 10.1016/j.chemosphere.2021.130984.

Auther information

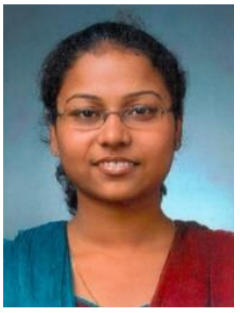

Deekshitha S. Nayak *completed Ph.D. in the Department of Electrical and Electronics Engineering in Manipal Institute of Technology, Manipal in the year 2022. Completed B. E (Electrical and Electronics) degree at YIT Moodbidri in the year 2014 and M. Tech (Electronics) degree at Canara Engineering College in the year 2016.The area of interest are Renewable Energy, Power Electronics, Motor and Drives.*

Dr. R. Shivarudraswamy*, working at Manipal Institute of Technology, Manipal, in the Department of Electrical & Electronics as an Associate Professor from last 15 Years, before worked in the Industry as an Electrical Maintenance Engineer about 3 and half years. Completed B. E (Electrical) degree at SIT Tumkur in year 1994 & M. Tech degree at Malnad College of Engineering in the year 2002 & completed Ph. D degree at NITK Surathkal, Karnataka in the year 2013. The area of research interest are Distributed Generators and Energy conservation and Management. Published many papers in the National & International Conferences & Journals.*

